AD-A034 089 MISSISSIPPI VALLEY STATE COLL ITTA BENA F/G 17/5
ELECTROREFLECTANCE, FARADAY ROTATION AND HALL EFFECT OF INFRARE--ETC(U)
JUL 76 S A KHAN, H PILLER N00019-74-C-0503
UNCLASSIFIED NL

1 OF 1
ADA034089

END

DATE
FILMED
2-77

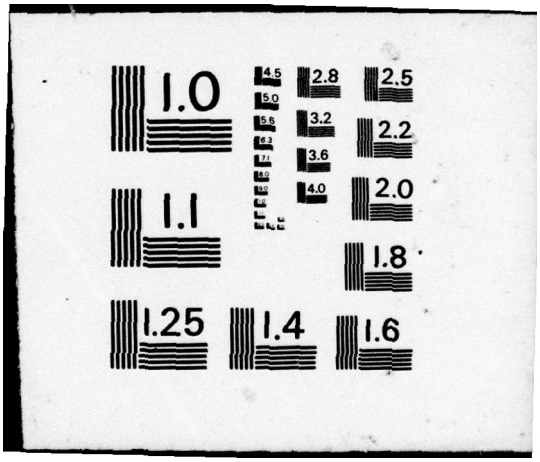
1.0
1.1
1.25
1.4
1.6
1.8
2.0
2.2
2.5
2.8
3.2
3.6
4.0
4.5
5.0
5.6

Contract No. N00019-74-C-0503

12 b.s.

Final Report

Electroreflectance, Faraday Rotation and Hall Effect of Infrared Detector Materials

July 1976

Prepared for

Naval Air Systems Command

(Dr. H. J. Mueller)

By

Mississippi Valley State University
Itta Bena, Mississippi 38941

(Dr. S. A. Khan)

and

Louisiana State University
Baton Rouge, Louisiana 70803

(Dr. H. Piller)

390 937 SC

Covering the Period

July 1974 to July 1976

Contract No. N00019-74-C-0503

Final Report

Electroreflectance, Faraday Rotation and Hall Effect of Infrared Detector Materials

July 1976

Prepared for

Naval Air Systems Command

(Dr. H. J. Mueller)

By

Mississippi Valley State University
Itta Bena, Mississippi 38941

(Dr. S. A. Khan)

and

Louisiana State University
Baton Rouge, Louisiana 70803

(Dr. H. Piller)

Covering the Period

July 1974 to July 1976

ELECTROREFLECTANCE, FARADAY ROTATION AND HALL EFFECT OF INFRARED DETECTOR MATERIALS

TABLE OF CONTENTS

Introduction

The alloy semiconductor $Pb_{1-x}Sn_xTe$ has a composition-dependent energy gap. The width of the energy gap is a linear function of the composition parameter x and can be expressed according to the relationship

$$Eg(x) = |(1-x)\ Eg(PbTe) - x\ Eg(SnTe)| \ .$$

PbTe and SnTe both have energy band extrema at the zone boundary in the (111) direction. The bands forming the extrema have the same symmetry in the two materials but their roles in relation to conduction and valence bands are reversed - the symmetry of the conduction (valence) band in PbTe corresponds to that of the valence (conduction) band in SnTe. Thus, when the two materials are mixed to form the $Pb_{1-x}Sn_xTe$ alloy system, at some value of the composition variable x the roles of the bands must interchange.[1] As the concentration of SnTe is increased in relation to that of PbTe, the bands approach together until the crossover composition of the alloy system is reached. A further increase in the value of x makes the bands diverge and increase the energy gap. This behavior is unique to the binary alloy semiconductor systems $Pb_{1-x}Sn_xTe$ and $Pb_{1-x}Sn_xSe$ in the Lead-Tin chalcogenide family and results in an alloy system in which any energy gap from zero up to that of PbTe(for example in PbSnTe) can in principle be chosen by a proper

choice of the composition parameter x. Alloys on the PbTe side have properties similar to PbTe with a positive temperature coefficient of the energy gap whereas alloys on the complimentary x side have a negative temperature coefficient of energy gap and properties similar to SnTe. A complexity in the band structure of the alloy system is introduced by a slight displacement of the extrema of both bands off the (111) axes from the L points. For values of the variable x in the neighborhood of the cross-over composition there is a distinct break in the temperature characteristics of resistivity. This corresponds to the change in sign of the temperature coefficient of the energy gap at the cross-over point.

The importance of the study of the Lead-Tin-chalcogenide alloy systems has been in their application for the detection of radiation in the 8 - 14 micrometer wavelength range. In this region there is a relatively transparent atmospheric window and also the peak infra-red emission of a $300^{o}K$ black-body occurs in this range. The lead-tin chalcogenide intrinsic detectors operate satisfactorily at temperatures near $77^{o}K$ which can be obtained with relative ease using the liquid nitrogen systems. In contrast, the extrinsic Germanium detectors require much lower temperatures and use of liquid helium becomes mandatory thus entailing more-complex cryogenic systems. PbSnTe detectors can be operated in the photovoltaic as well as in the photoconductive modes. However, for all

detector applications, the carrier concentrations must be relatively low (well below $10^{18}/cm^3$). Because of the very low values of the effective mass, average or above average values of the carrier concentration shift the absorption edge to higher energies due to the filling of the bands. Therefore a study of the material characteristics after it has been annealed is more responsive of the detector application development program. The refractive index of PbSnTe is comparable to that of PbTe which is quite large. As a result a single reflection from the detector surface produces a loss of about 50% in the signal strength of the incident radiation. In the photovoltaic mode a very fast response is obtained. This feature in combination with the high detectivity characteristics makes PbSnTe detectors of value for use with the 10.6 micrometer carbon dioxide lasers.

The characteristics of the Lead-Tin chalcogenide systems are sensitive to the values of the composition parameter x. The knowledge of microscopic parameters deduced from the combined electrical and optical properties of the alloy system provides sufficient information for the improvement of the growth techniques of the alloy and also for the improvement of the performance of the infrared detector. The detectivity and spectral response of a detector are connected with values of the carrier concentration, carrier mobility, effective mass, the composition of the alloy

system, and hence the energy band structure of the material. The measurement of electro-reflectance[2] provides a powerful technique for the investigation of the band structure of a material. It enables the critical point energies of inter-band transitions to be located under conditions in which the absorption coefficient is too high for transmission measurements to be practical, i.e., at photon energies well above the absorption edge. This technique has the practical advantage that the electric field need only be applied to a surface layer of the semiconductor under investigation. However, conversely, only the properties of the surface are measured. This may be regarded as a disadvantage when the investigation of the characteristics of the bulk is to be made. The measurements are performed by modulating the surface barrier field of the sample with an external alternating voltage. It is usual to make measurements with various d.c. biases superimposed on the modulating field, thereby varying the average value of the field. If the varying component of the reflected intensity is detected with a lock-in amplifier, then it is possible to measure very small fractional changes $\Delta R/R$ in the reflectivity of the specimen. This fraction exhibits peaks at photon energies very close to the critical points. By monitoring the shift of the peaks of electroreflectance with change in the values of the d.c. bias, it becomes possible to distinguish between peaks due

to parabolic edges and those due to saddle-point edges of the joint density of states characteristics. A series of electro-reflectance oscillations should in principle be observed at or near each critical point. However, lifetime broadening due to carrier scattering effects damp out the periodic structure so that only a single peak is usually observed. The position of the aggregated peak would be expected to deviate from the energy of the critical point by less than the half-line width. The characteristics of the Lead-Tin chalcogenides are significantly affected by extrinsic perturbations. The absorption edge is shifted to shorter wavelengths when the material is n-type and is heavily doped. This so-called Burstein-Moss shift plays an important role in the spectral response of the narrow gap semiconductors like $Pb_{1-x}Sn_xTe$ since the effective mass is quite small as is the energy gap.

In the present report we describe the experimental procedures and results of electroreflectance and Hall effect measurements. The Hall effect and conductivity measurements were performed on a rectangular parallellopiped sample of $Pb_{0.8}Sn_{0.2}Te$ of satisfactory geometry. The electroreflectance of PbTe and $Pb_{0.8}Sn_{0.2}Te$ has been measured by using the electrolyte technique as well as the metaloxide semiconductor (MOS) configuration. These measurements provide means for the determination of the distribution of carrier concentration

in the $Pb_{1-x}Sn_xTe$ samples. For that purpose, the MOS configuration is the most convenient in high conductive materials like $Pb_{1-x}Sn_xTe$. The information obtainable from the carrier distribution measurements is useful for the improvement of the growth techniques of the infrared materials.

Single crystals with excellent homogenity and good quality of $Pb_{1-x}Sn_xTe$ are relatively easily produced.[3] This fact and their optical properties have made these alloys particularly useful for infrared detectors as well as lasers.

The purpose of this research is to obtain the knowledge of microscopic parameters in ~~this alloy system~~ the ALLOY SEMICONDUCTOR Pb(1-x) Sn(x) Te from the combined electrical and optical properties. Studies of the surface properties and the optical properties will provide information which will lead to an improvement of the performance of infrared detectors and laser devices.

Band Structure

The problem of detailed crystal calculations is a formidable one in the case of narrow band gap semiconductors due to the fact that the accuracy is far from the required one. For the understanding of the band gap change for elements and compound sequences such as lead telluride and tin telluride, the impact of the relativistic shifts appear decisive in first principle calculations of the band structures of the materials.[4]

The characterization of the energy gap law has been performed by using opto-electronic effects, such as electro-

luminescence and photovoltaic detection, in p-n junctions. In the lead-tin-selenide-alloys photovoltaic effects have been observed on each side of the zero gap transition showing a substantial difference with respect to other narrow gap semiconductors. The energy gap of lead-tin telluride alloys as a function of x has been measured by I. Melngailis,[5] using laser emission and photovoltaic effects, but only for x smaller than x_0 at 12^oK and 77^oK.

For the lead salts, the electronic states of interest are L_6^+ and L_6^- which have only a two-fold spin degeneracy. The alloy can be a narrow band gap semiconductor on both sides of the $L_6^+ - L_6^-$ crossing and exhibits a semiconductor-semiconductor transition.

Due to the positive value of the band gap deformation potential of the alloys with lead salt-like band structure, extention to smaller gaps under hydrostatic pressure can be expected. During the last years a lot of studies were undertaken on the narrow band gap semiconductor alloy lead-tin-telluride system. A large number of papers dealt with optical data, classical and quantum transport property measurements and also the evidence of an anamolous behavior of elastic constants at a crossover point. More and more accurate characterization measurements are continuing and this is of crucial importance for the question of the attainability of the zero gap.

Faraday Rotation

During the last decade an extensive study of the Faraday rotation in semiconductors has been made as a means of obtaining energy band parameters and of investigating different dispersive mechanisms.[6]

Two basic mechanisms are responsible for the Faraday rotation observed in semiconductors: a) a positive free carrier rotation which is the dispersive consequence of the cyclotron resonance of the conduction electrons, and b) an interband contribution which arises from the dispersion of all interband magneto-optical transitions.

The interband effect is strongly dependent on the spin spreading of the Landau states; the relative sign of the combined valence and conduction band g-factors determines the sign of the rotation. The effects are separable primarily due to the photon energy dependence. Measurements of the free carrier Faraday rotation have been used to give good determinations of the electron effective mass as a function of the carrier concentration and temperature, and have been particularly useful in semiconductor compounds where the conduction band minima are not at $k = 0$.

Owing to its ease of measurement in the transparent region of the crystal below the forbidden energy gap, non-resonant interband Faraday rotation has also attracted a large amount of experimental and theoretical interest. In the last few years several studies were made of the dependence

of the interband effect on free electron concentration,[7,8,9] and temperature.[10] Also, Mitchell et al.[11] have reported the observation of one oscillation in the nonresonant interband Faraday rotation of lead salts as a function of magnetic field. From the application of simple band theory, they obtained a good estimate for the carrier concentration of the sample. The problem of interband transitions in lead telluride can be treated on the basis of single non-degenerate conduction- and valence bands. These split into normal Landau subbands under the action of a magnetic field but require the inclusion of spin characterized by conduction- and valence band g-factors.

The selection rules for interband transitions between these simple bands have been found by Burstein, et al.[12] to be that the change in Landau quantum number $\Delta n = 0$, and spin quantum number $\Delta m_j = \pm 1$ while $\Delta k_c = 0$. The latter implying vertical transitions with momentum conserved. The transitions corresponding to changes of $\Delta m_j = \binom{+1}{-1}$ occur for $\binom{\text{left}}{\text{right}}$ circularly polarized modes of radiation respectively. Since the matrix elements for both transitions are the same for all values of n, that is, the probabilities are the same for both left and right circularly polarized transitions, the energy denominators in the following Eq. (1), which has been formulated by both Boswarva et al. and Bennet and Stern,[13] yield essentially the result for the rotation θ:

$$\theta = \frac{\omega}{2c}(n_+ - n_-) = \frac{-e^2}{4nc\hbar\epsilon_o} \sum_k^o \sum_{k'}^u \frac{\omega^2}{\omega_{k'k}^2} \frac{[|V_{k'k}(+)|^2 - |V_{k'k}(-)|^2]}{\omega_{k'k}^2 - \omega^2} \qquad (1)$$

in mks units. The summations over $V_{k'k}(+)^2/\omega_{k'k}^2 - \omega^2$ and $V_{k'k}(-)^2/\omega_{k'k}^2 - \omega^2$ express mathematically the total interband, i.e., bound electron contribution to the squares of the refractive indicies for right circularly polarized modes (n_+^2) and left circularly polarized modes (n_-^2); where n is the average refractive index and V($\pm$) are the electron velocity operators for the two modes of radiation. The sum over k is over all occupied one-electron states and the sum over k' is over all unoccupied states.

At long wavelengths where the radiation frequency ω tends to zero, θ is proportional to ω^2. It can be seen from Eq. (1) that the total Faraday rotation is determined by a balance between two large terms arising from the contributions from absorptions of right and left circularly polarized waves. Since the matrix elements for both transitions are the same for all values of n, the energy denominators in Eq. (1) would be expected to give a larger polarizability for transitions of smaller energy. As the observed interband rotation PbTe is negative, for applied radiation of energy near the energy gap the contributions from right circularly polarized radiation transitions are greatest. The physical significance of this is that the average conduction and valence band g-factors must be negative. Experiments on samples of PbSnTe

having different carrier concentrations should enable quantitative association of the levels involved with definite values of n and spin quantum numbers to be made, and detailed information of band-structure parameters obtained. The variation of the distribution of magnetic states near the Fermi level provides a sensitive method of perturbing the balance between contributions to the overall Faraday rotation from right and left circularly polarized components and gives rise to oscillations in the interband rotation at low temperatures. By analogy with the de Haas-van Alphen effect these oscillations allow quantitative determinations of useful band structure parameters.

The measurement of interband and free carrier Faraday rotation together will yield the parameters m* (effective mass), the g values and the Fermi level of PbSnTe. The analysis shows that the Faraday rotation can provide a quantative method for such determinations. This method could be particularly useful since it includes an optical method for determining the position of the Fermi level. This technique can also be used in samples with larger impurity concentrations in which more direct measurements like cyclotron resonance cannot be observed.

The observation of anisotropic effects in highly doped crystals could be useful and it is planned to study the

interband rotation as a function of the crystal orientation.

The study of interband rotation in p-type materials should yield analogous information on valence band parameters. Only one preliminary study of the Faraday rotation in PbSnTe has been published.[14]

No low temperature interband Faraday effect has been reported in the literature. The authors determined the Faraday rotation spectra at 90, 120, and 295°K for samples with carrier concentrations larger than $8 \times 10^{16}/cm^3$.

A most recent review of the magneto-optic Faraday effect in semiconductors including the IV-VI compounds PbTe and PbSe was given by Ukhanov.[15]

The samples for our measurements cover a carrier concentration range from 10^{15} to $10^{18}/cm^3$ in the n- and p-type. The samples were cut from single crystals grown by the Bridgman method. Before measurements, the samples were treated in a polishing etchant and the contacts were deposited using a method described in Ref. 14. The transport effect (electrical resistivity and the Hall coefficient R) have been measured in the temperature range from 4.2 to 460°K. It is known that the valence band of PbSnTe is complex and consists of light hole and heavy hole bands. At low temperatures and low densities the holes are concentrated in the light hole band. In this case the temperature and carrier density dependences of the transport

coefficient can be described by a one-band model.[16] The Hall coefficient increases with increasing temperature. This behavior can be explained by transfer of holes to the heavy hole band whose top lies below the light hole band in this range of temperatures. The light hole band is displaced downward with rising temperature.[17] The occupancy of the heavy hole band also increases with the hole density. Therefore, the maximum of the Hall coefficients R_H of the samples with higher hole densities are shifted towards lower temperatures. The temperature dependence of R_H is similar to that observed in the presence of an impurity band.

OPTICAL MEASUREMENTS

Sample Preparation

As-grown p-type PbTe and p-type $Pb_{0.8}Sn_{0.2}Te$, supplied by Dr. R.A. Chapman, Texas Instrument Co., were used as samples.

These samples were lapped with either Alundum on a polishing cloth (AB Microcloth, Buehler Ltd.) or 600 Grit Carbimet Paper discs (Buehler Ltd.). The final lapping was made with fine optical Jewelers Rouge (Edmund Scientific Co.) in distilled water, to produce mirror-like surfaces.[18] Chemical polishing with the solution[19] 20 gram KOH, 45 ml H_2O, 35 ml glycerol and 20 ml ethanol was used.

Both PbTe and $Pb_{0.8}Sn_{0.2}Te$ were etched in the following solution[20]: KOH (saturated at 20°C) 10 volume, H_2O_2 with a 2-3 volume and ethylene glycol 10 volume at 25°C. The degree of stirring the solution and the amount of bubbles produced by H_2O_2 are critical parameters for etching.

MOS Samples

The aluminum oxide (Al_2O_3) films were evaporated by using an electron gun in the high vacuum system of the optics laboratory at LSU (see picture 1).

The electron gun system with cold trap, diffusion pump, and forepump is initially pumped down to the mid 10^{-7} Torr range. Chips of optical grade Al_2O_3 (Materials

Research Corporation) are placed into an intermetallic composite ($BN-TiB_2$) crucible and are evaporated with the 6 kW electron beam gun. An electron gun power supply, model ES-6 of Airco Temescal Division, was used. The electron gun is operated with the power of the beam ranging between 300-500 Watts with the emission current ranging between 30 mA-50 mA and a fixed acceleration potential of 10 kV. The power levels yield a deposition rate of 100-600 Å/min. at a distance of 30 cm between source and substrate. The pressure during evaporation varied between 4×10^{-6} and 10^{-7} Torr.

MOS samples with Al_2O_3 film thickness of 600 Å, 700 Å, 1000 Å, and 1500 Å were produced. These films were measured with a thickness monitor (Sloan model DTM-4). Very small deposition rates do not give good oxide films for our purpose. Semitransparent films of Ni were evaporated as an electrode with sheet resistances between 400 Ω/sq. and 2200 Ω/sq. The area of the Ni electrode was 3 mm x 5 mm., Deviations from the flatness of the $Pb_{1-x}Sn_xTe$ surface do not affect the breakdown voltage of the oxide. Small holes made in the lapping process and etch pits and scratches enhanced by etching, did not change the MOS-sample characteristics. The electrical contact is made directly to the Ni film by using a thin gold wire and Dupont No. 4817 silver paint.

Optical System

A model 218 monochromator (McPherson Instrument Corporation) was used in combination with a Tungsten light source and a photomultiplier (model E.M.I. 9558-QA) as a detector. (See Picture 2)

A block diagram of the experimental set-up is shown in Fig. 1. The electric field is created at the $Pb_{1-x}Sn_xTe$ sample surface with a 450 Hz square wave. Continuity of the sample contacts can be verified by observing a slight rounding and decrease of the amplitude of the wave on the oscilloscope when connection to the sample is made.

As a wave generator, a Wavetek model 113 was used. This generator allows independent variation of modulation amplitude and dc bias and also provides a variety of waveforms, making it very convenient to the ER* measurement on MOS samples.

In order to obtain the ratio of ac to dc component of the ER signal $\Delta R/R$, the electronic servo controlled power supply (PAR Model 280) was used. This power supply controls the high voltage applied to the photomultiplier so as to keep the dc output constant. The output from the lock-in amplifier, which measures the modulation of reflectivity, is proportional to $\Delta R/R$ if the dc output is kept constant. One can get the absolute value of $\Delta R/R$ by calculating the appropriate scaling factor.

* Electroreflectance

A photometric amplifier (PAR Model 221) was used as a preamplifier. The dc output was kept at approximately 5 V.

Cryostat and Sample Mounting

To prevent the reflected light of the window from getting to the photomultiplier, the MOS sample was mounted on the copper cooling finger in the cryostat at a slight angle with respect to the quartz window of the cryostat. The cryostat was evacuated by a sorption pump and an ion pump (Consolidated Vacuum Corporation Type PDV-2-A) to the 10^{-7} Torr vacuum range.

MOS ELECTROREFLECTANCE DATA

Electroreflectance of PbTe

In the first study we were concerned with the E_1 structure at photon energy of approximately 1.2 eV.* Since the Al_2O_3 oxide layer and Ni semi-transparent film have good transmission to at least 7 eV,[21] it was possible to study structures attributed to higher interband transitions of these materials. Figure 2 shows the ER of p-type PbTe for applied square wave voltage +6 V/-38 V which means 44 V peak to peak square wave voltage with a dc bias of -16 V. The thickness of the Al_2O_3 film of this sample is 1500 Å. Two structures which show typical line shape in ER can be observed at 2.2 eV and 3.3 eV in the 1.0 - 4.5 eV range. The location of the peak at 2.2 eV is in excellent agreement with the ER data using the electrolyte method by Aspnes and Cardona.[22] They have analyzed this structure and assumed it to be attributed to the interband transition $\Delta_7(1) \rightarrow \Delta_6(5)$[23] in the (100) direction in the Brillouin zone. Bogacki et al.[24] have measured thermoreflectance of PbTe and found the peaks at 2.35 eV, assigning it to be E_2 structure. This has also been observed at 2.4 eV in the reflectivity measurement.[25] In the energy band calculation by Lin and Kleinman[26] it was found that the energy gap

---

* The notation used here is that originally introduced by Cardona and co-workers (see CARDONA, M. et al., Phys. Rev. 154, 696 (1967)).

corresponding to $\Delta_7(1) \rightarrow \Delta_6(5)$ is 2.58 eV. One may recognize that this structure can be used for measuring the distribution of carriers in the sample, if in fact it is true that this structure can be attributed to the transitions on the Δ symmetry line. In this case the ER is not affected by Fermi level transitions[27] and satisfies the low field condition in ER as described in the first technical report (technical report covering the period July 1, 1974 - October 31, 1974).

The structure found at 3.3 eV seems to correspond to the E_3 transition ($\Delta_6(4) \rightarrow \Delta_6(6)$) which has been found in the reflectivity measurements by Conlin[28] at 3.5 eV and by Berolo[29] at 3.48 eV. This transition edge has been assigned to the M_2 critical point by the energy band calculation by Lin and Kleinman. Their theoretical value of the gap is 3.36 eV. This theoretical value is therefore in excellent agreement with the present results. It may be pointed out that this structure is also useful for the measurement of the distribution of carriers in PbTe samples.

We were unable to obtain the signal of ER at low temperature. We assume that it has been caused by partial breakdown of the Al_2O_3 film.

ER of PbSnTe

Figure 3 shows ER of p-$Pb_{0.8}Sn_{0.2}Te$. In this signal we may observe two main structures. One is found in the

photon energy range from 1.8 eV-2.5 eV, with a shoulder at approximately 2.0 eV. This shoulder was not observed in PbTe. The other structure is in the 2.7 eV-3.5 eV region with a peak at 3.1 eV. It is difficult to make an assignment to the structure with the shoulder at lower photon energy from the present status of our data. It would be reasonable, however, to assign the peak at 2.3 eV as a structure due to the E_2 transition ($\Delta_7(1) \rightarrow \Delta_6(5)$), as far as its location of the photon energy is concerned. These results suggest that the energy gap in the E_2 transition increase with the alloy composition x in the $Pb_{1-x}Sn_xTe$ alloy system. On the other hand, Berolo[29] found in his reflectivity measurement of $Pb_{1-x}Sn_xTe$ that the energy gap decreased monotonously with x. He estimated the energy gap of the E_2 transition to be 2.2 eV. This is very close to the value we have obtained from our data. Concerning the shoulder, further experiments are required to recognize whether it is due to the subsidiary oscillations of the E_2 structure or due to effects of another transition.

The structure in the higher photon energy region, with its peak at 3.1 eV (see Fig. 3) corresponds to the E_3 structure at 3.3 eV in ER of PbTe in Fig. 2. This value of energy gap of $Pb_{0.8}Sn_{0.2}Te$ suggests that the energy gap decreases with x. The line shape is much broader than that of PbTe due to the alloy broadening effect as described in the first report.

Discussion

We now discuss the assignment of the structure observed at 2.2 eV in the ER signal of PbTe using the electro-optical theory as described in the Appendix.

Recently Berolo developed his theory of electroreflectance with MOS configuration in GaAs.[29] He found that the electroreflectance spectra are altered by various parameters, such as the refractive index and the thickness of the film layers. He demonstrated that for layers of oxide films with a thickness of $\lambda/2$ (70% transmitting films) there was no detectable difference between the ER spectra of the MOS sample and the ER spectra of samples without the double (Ni and oxide) layers.

In the present measurement, the thickness of Al_2O_3 was 1500 Å which is nearly equal to the $(1/4)\lambda$. Here λ is around 5800 Å close to the E_2 structure in PbTe. When the oxide film thickness is $(1/4)\lambda$, the line shape of the ER spectra changes in its phase by $(3/2)\pi$, in terms of Aspnes low field spectra.[30]

The ER spectra of MOS samples are shown in Fig. 4, d_o and d_m are the thickness of oxide film and Ni film, respectively. One can see that the spectrum we are concerned with in Fig. 2 resembles the spectrum in Fig. 4(b), therefore the "real" spectrum which is not affected by the double layers would be expected to be the one in Fig. 4(a). Preliminary computer studies which are in progress tend to prove this assumption.

In general the field induced change in reflectively $\Delta R/R$ is described with the field induced change in dielectric constant (see Appendix).

One can see immediately from the Figs. A-1 and A-2 that $\Delta R/R$ at 2 eV of PbTe mostly consists of $\Delta\varepsilon_2$, the imaginary part of the change in dielectric constant. It turns out, therefore, that the ER spectrum of Fig. 4(a), which swings down and up and has the value of energy gap near the middle of the two large peaks, is determined only by $\Delta\varepsilon_2$.

By comparing the spectra in Fig. A-2 and Fig. 4(a) it can be recognized that the observed spectrum at 2.2 eV corresponds to the one having an M_2 type critical point.

As far as the energy location of the transition is concerned, the location of the structure in our present data ($\simeq$2.2 eV) is the closest to the transition energy of $L_3^{45}\rightarrow L_{3'}^{45'}$. However, the type of the critical point at which this transition takes place is $M_0 + M_1$ according to the energy band calculation.[26] The second closest value can be found in the transition of $\Delta_7(1)\rightarrow\Delta_6(5)$ which has the M_2 type critical point.

In conclusion, we assign the structure around 2.2 eV of PbTe to be due to the transition $\Delta_7(1)\rightarrow\Delta_6(5)$. This has the M_2 type of critical point, and we can be sure again that this spectrum can be utilized to measure the distribution of carrier concentration without worrying about the effect of the Fermi level transition.

Summary

(1) The electron gun evaporation system built recently can reach 4×10^{-7} Torr before evaporation and 10^{-6} Torr range during evaporation. MOS samples have been successfully fabricated using this system.

(2) ER of PbTe and $Pb_{0.8}Sn_{0.2}Te$ have been measured in the photon energy region from 1.5 to 4.5 eV in the MOS configuration at room temperature. Two structures of ER of PbTe have been found in this photon energy range and have been assigned to be due to the transitions $\Delta_7(1) \rightarrow \Delta_6(5)$ and $\Delta_6(4) \rightarrow \Delta_6(6)$, respectively. This indicates that they can be used for the measurement of distribution of carrier concentration. The signals of $Pb_{0.8}Sn_{0.2}Te$ show similar structure as those of PbTe except that they have broader structure and an unknown shoulder in the E_2 structure.

HALL EFFECT MEASUREMENTS

Laboratory Set-Up

As a support to the work going on at Mississippi Valley State University on the Navy Project, Research Corporation had awarded $10,700 to purchase some needed equipment. Following items have been purchased under this grant:

1 - PAR Model 186 Lock-in-Amplifier

1 - WALKER/MAGNION Model HV4W1 Electromagnet

1 - WALKER/MAGNION Model RS-245B
Electromagnet Power Supply

1 - AIR PRODUCTS CYRO-TIP System

1 - ORIEL CORPORATION Grating
Monochromator with 2, 4, 8, 12 Micron gratings
and two drive mechanisms

2 - PbS detectors

2 - PbSe detectors

1 - 1.1 mi-ron long pass filter

1 - 2.6 micron long pass filter

1 - 6.3 micron long pass filter

One Hewlett-Packard Model 7004B X-Y Recorder with 17172A Time Base and 17171A D.C. Pre-amplifier modules has been purchased on the NAVY contract.

In addition, items in the laboratory include the following:

1 - Leeds and Northrup Potentiometer

1 - Keithley Model 155 Micro-volt Null Detector

1 - Kepco d.c. programmable current supply

2 - Laboratory Oscilloscopes

1 - Spectra Physics Laser

All this equipment has been tested and the laboratory has been set up to make Hall effect and Resistivity measurements on PbSnTe Samples. The magnet power supply is hooked up to a 3-phase, 220 volt power source and the magnet has been calibrated on a gap of one inch using a standard Hall Probe. Fig. 5 shows the calibration curve of the magnet. The magnet gives a fairly homogeneous field of 9 kg without saturation at this gap value.

Low Temperature Set-Up:

Air Products Model AC-1 CRYO-TIP is a miniature open-cycle Joule-Thomson refrigerator that produces liquid nitrogen in an evacuated cavity. Temperature dependent phenomena down to liquid nitrogen temperature can be investigated for a variety of applications using this device. The schematic for a typical CRYO-TIP system is shown in Fig. 6. The basic components of this system are:

Heat Exchanger

Gas Control Panel

Flexible Gas Lines

High Pressure Regulator

Vacuum Shroud

The CRYO-TIP cooling device has been assembled and tested. This nitrogen-operated Joule-Thomson device goes down to liquid nitrogen temperatures with precise temperature control. The whole operation of cooling down from the room to the nitrogen temperature takes about 10 minutes.

Measurements of Hall Effect and Resistivity in PbSnTe

Resistivity and Hall Effect measurements have been performed on a sample of PbSnTe at room temperature. A 15.3 mm x 4.9 mm x 1.3 mm rectangular sample of PbSnTe has been prepared and mounted on the tip of a stainless steel dewar. We present below a discussion and analysis of the Hall effect and resistivity data.

Common techniques of Hall effect and resistivity measurement put serious limitations on sample geometry and current and voltage contacts in order to be meaningful. The voltage drop across a semiconductor sample carrying an electric current always contains unknown metal-semiconductor contact potentials. The seriousness of these limitations is relaxed by using a method of measurement by Van der Pauw.[34] In this technique, the sample can be of arbitrary shape. If along the perimeter of a plane parallel plate of thickness d, four point contacts A,B,C,D are attached, and for a current I_{AB} from A to B there is a voltage drop V_{CD} between the points C and D, then we can define a quantity

$$R_{AB,CD} = |V_{CD}|/I_{AB}$$

By permuting the arrangement would yield similarly

$$R_{BC,DA} = |V_{DA}|/I_{BC}$$

It was shown by Van der Pauw that the resistivity ρ of the sample is given by

$$\exp(-\pi \frac{d}{\rho} R_{AB,CD}) + \exp(-\pi \frac{d}{\rho} R_{BC,DA}) = 1 . \qquad (1)$$

By defining a factor f by the relation

$$\rho = \frac{\pi}{\ell n 2} d \frac{R_{AB,CD} + R_{BC,DA}}{2} f , \quad d = \text{Thickness} \qquad (2)$$

the above relation yields

$$\cosh \{ \frac{\ell n 2}{f} \frac{R_{AB,CD}/R_{BC,DA}-1}{R_{AB,CD}/R_{BC,DA}+1} \} = \frac{1}{2} \exp (\frac{\ell n 2}{f}) \qquad (3)$$

which can be solved for the ratio

$$R_{AB,CD}/R_{BC,DA}$$

By making two resistance measurements at the same sample one can estimate f by an interactive process using Exp. (3). A substitution of this value of f in Eq. (2) gives the resistivity value.

For a Hall measurement the arrangement would be to measure voltage between alternate points B and D for a current I_{AC} between points A and C. The resistance is written

$$R_{AC,BD} = V_{BD}/I_{AC}$$

When a magnetic field B is applied normal to the sample surface, the resistance is changed by amount $\Delta R_{AC,BD}$ and the Hall coefficient is obtained by the relation

$$R_H = \frac{d}{|B|} \Delta R_{AC,BD} \qquad (4)$$

We have used Eqs. (2), (3), and (4) to obtain R_H and ρ. From a knowledge of the magnetic field B and the current I, these values have been used to estimate the carrier concentration and Hall mobility. For B = 2.8 kG

$$\Delta R = \frac{\Delta V}{I} = \frac{14 \times 10^{-6}}{150 \times 10^{-3}} \frac{\text{volt}}{\text{Amp}}$$

$$R_H = \frac{d}{B} \Delta R = \frac{0.13}{2800} \times 10^{-3} \times \frac{14}{150} \frac{\text{volt x cm}}{\text{Amp x Gauss}}$$

$$= \frac{0.13 \times 14}{28 \times 15} \times 10^{-6} \times \frac{1}{10^{-8}} \frac{\text{volt x cm}}{\text{Amp x Wb/Cm}^2}$$

$$= \frac{13}{30} \frac{\text{ohm}}{\text{Wb}} \times \text{cm}^3 = 0.43 \text{ Coul x cm}^3$$

The carrier concentration is given by

$$n = \frac{1}{eR_H} = \frac{1}{1.6\times10^{-19} \times 0.43} \text{ per cc}$$

$$= 1.2\times10^{19}/cm^3$$

For an estimated value of f = 0.98 we can calculate

$$\rho = \frac{\pi}{\ell n 2} d \frac{R_{AB,CD} + R_{BC,DA}}{2} f$$

$$= \frac{\pi d}{\ell n 2} \times \frac{225\times0.98\times10^{-3}}{2\times150} \frac{\text{Volt}}{\text{Amp}}$$

$$= \frac{3.14\times0.13}{0.693} \times \frac{225\times10^{-3}}{300} \times 0.98 \ \Omega \text{ cm}$$

$$= 4.4\times10^{-4} \ \Omega \text{ cm}$$

The conductivity

$$\sigma = \frac{1}{\rho} = pe\mu_p$$

where p is the carrier concentration, e the electronic charge, and μ_p the mobility

$$\mu_p = \frac{1}{\rho Pe} = \frac{1}{4.4 \times 10^{-4} \times 1.4 \times 10^{19} \times 1.6 \times 10^{-19}}$$

$$= 1.014 \times 10^3 \frac{cm^2}{\text{volt x sec}}$$

Computer calculations:

In order to calculate the resistivity ρ from the relation

$$\rho = \frac{\pi}{\ell n 2} d \frac{R_{AB,CD} + R_{BC,DA}}{2} f$$

one must estimate the value of f from the relationship

$$\cosh \left\{ \frac{\ell n 2}{f} \cdot \frac{R_{AB,CD}/R_{BC,DA} - 1}{R_{AB,CD}/R_{BC,DA} + 1} \right\} = \frac{1}{2} \exp\left(\frac{\ell n 2}{f}\right)$$

by an interactive process on the computer. For the purposes of the present report, we chose a value of f that satisfies this relationship within a tolerable error limit and then using this value of f, have obtained the resistivity. However, for precise results, f must be obtained by an iterative procedure with substituted values of the measured quantities $R_{AB,CD}$ and $R_{BC,DA}$. It is proposed to obtain f by iteration after more precise measurements of $R_{AB,CD}/R_{BC,DA}$ are available.

FIGURE CAPTIONS

Fig. 1 Block diagram of the experimental setup.

Fig. 2 Electroreflectance of PbTe at room temperature with a modulation square wave voltage of +6 V/-38 V.

Fig. 3 Electroreflectance of $Pb_{0.8}Sn_{0.2}Te$ with a modulation square wave voltage of +4.5 V/-4.5 V.

Fig. 4 (a) Electroreflectance line shape without layers on the sample surface.

(b) Electroreflectance line shape with an oxide film thickness of $(1/4)\lambda$.[29]

Fig. 5 Calibration curve of the magnet with 1" pole-gap.

Fig. 6 Block diagram of the CYRO-TIP cooling system.

Fig. A-1 α and β of PbTe.[22]

Fig. A-2 Theoretical change of the real ($\Delta\varepsilon_1$) and imaginary ($\Delta\varepsilon_2$) parts of the dielectric function in an applied electric field for the six different cases of critical points.[33] The dashed curves are unbroadened. The solid curves correspond to a broadening parameter = 0.5.

Fig. A-3 Annealing heater circuit control to anneal PbSnTe crystals.

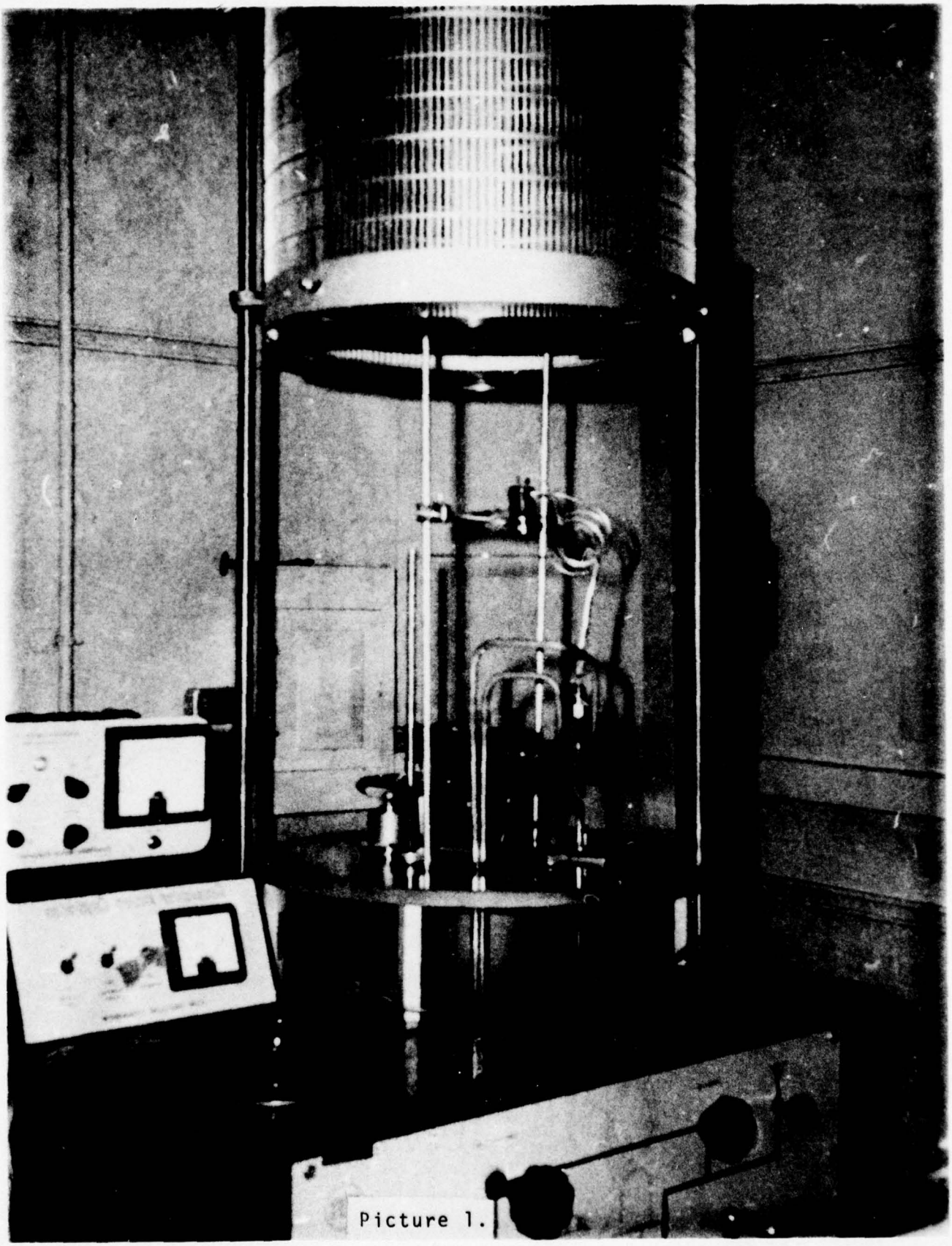

Picture 1.

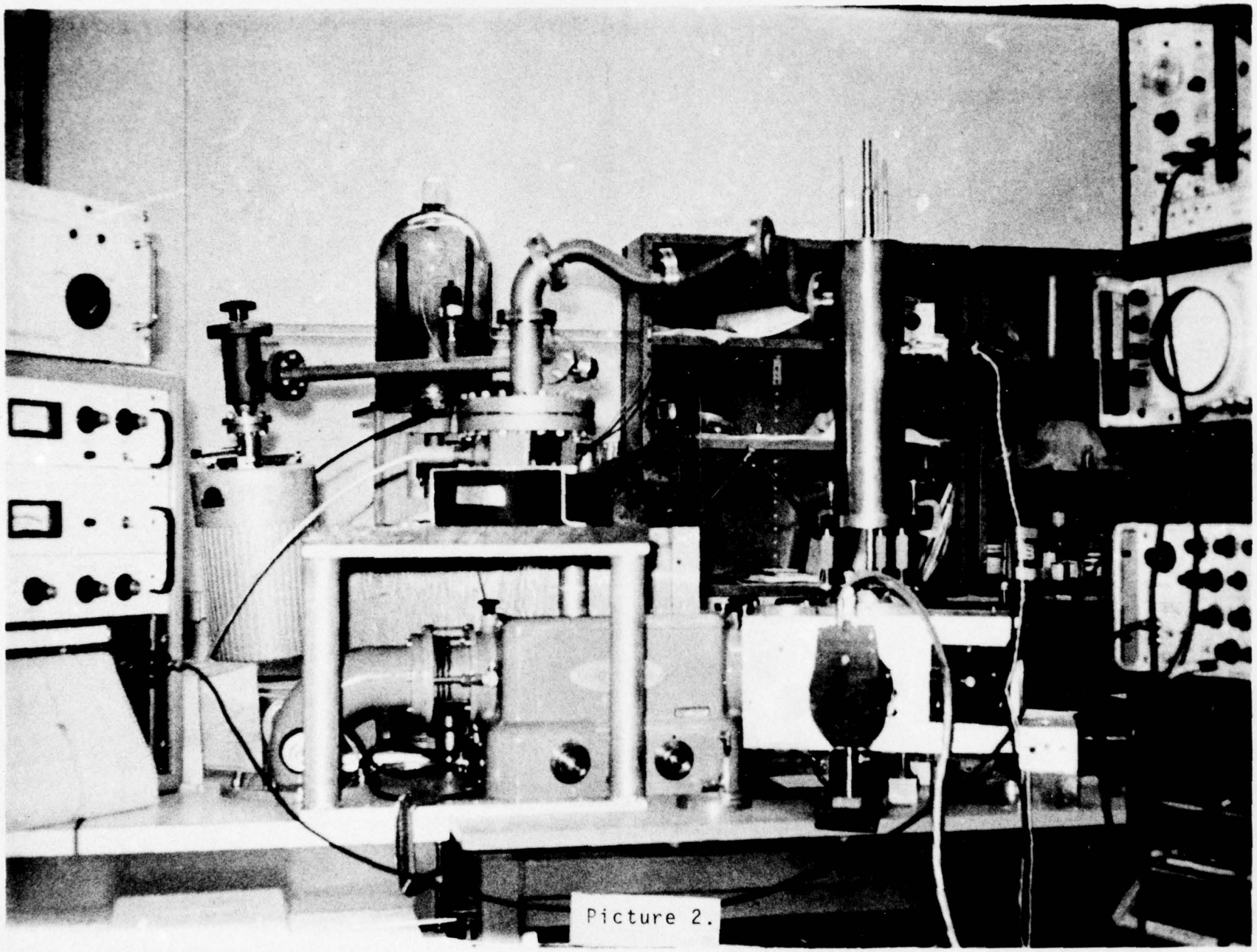

Picture 2.

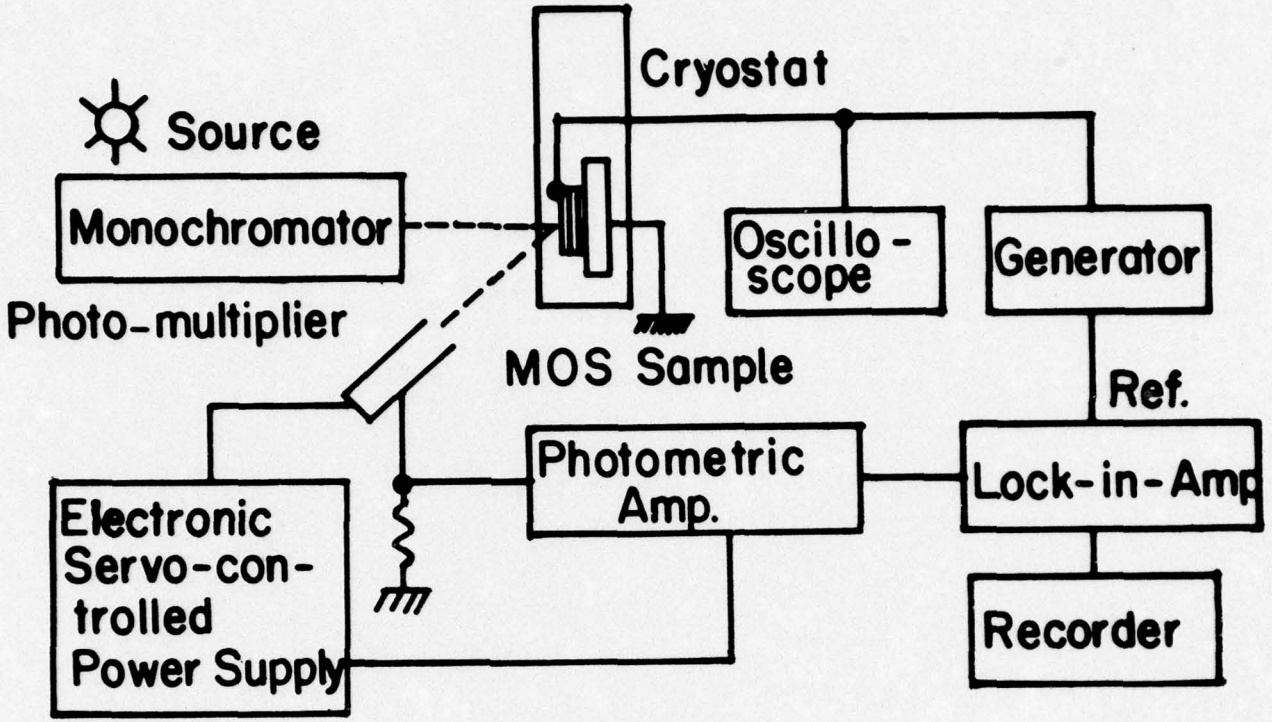

Fig.1. Block Diagram of the Experimental Setup.

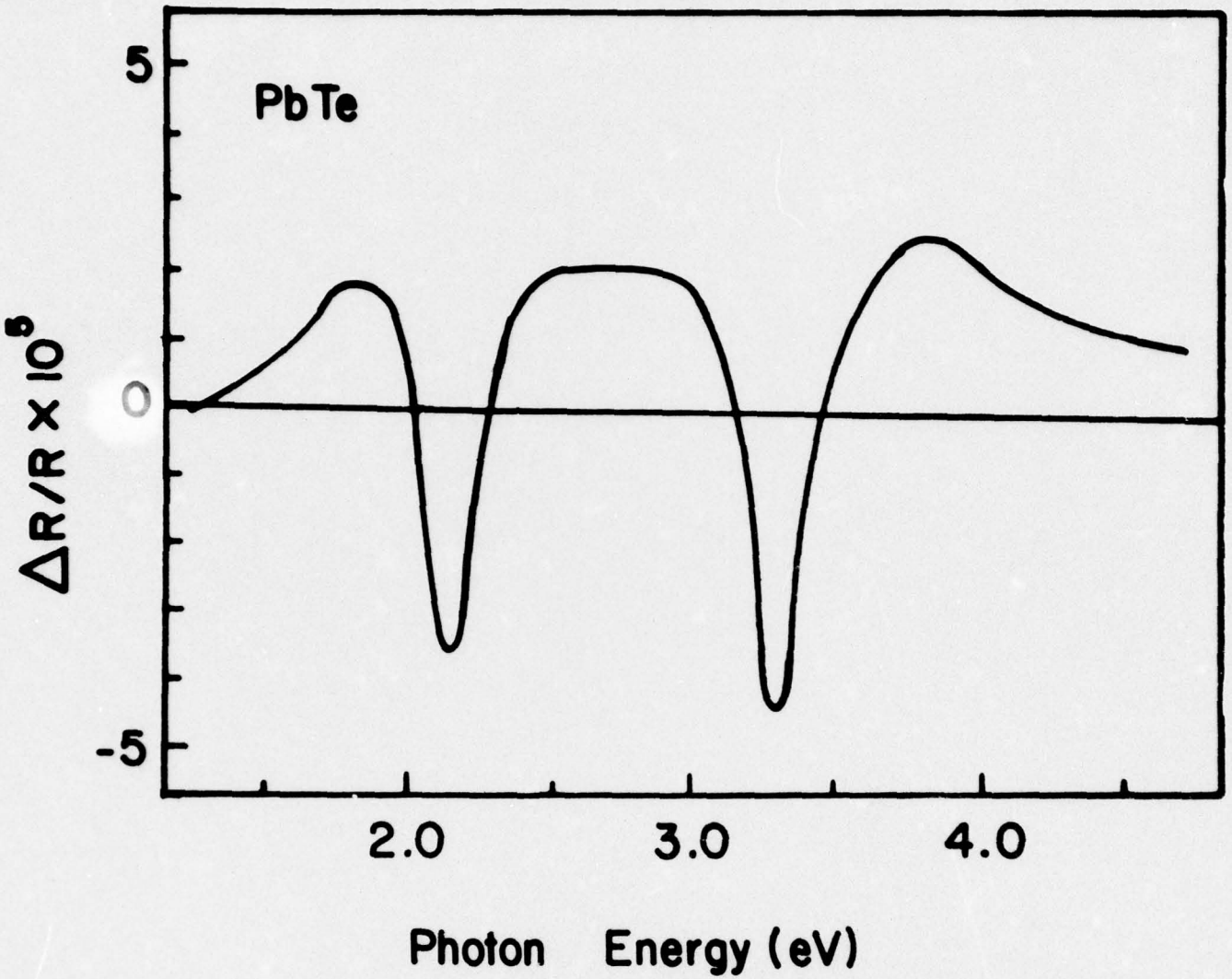

Fig.2. Electroreflectance of PbTe at Room Temperature with a Modulation Square Wave Voltage of +6 V/-3E V.

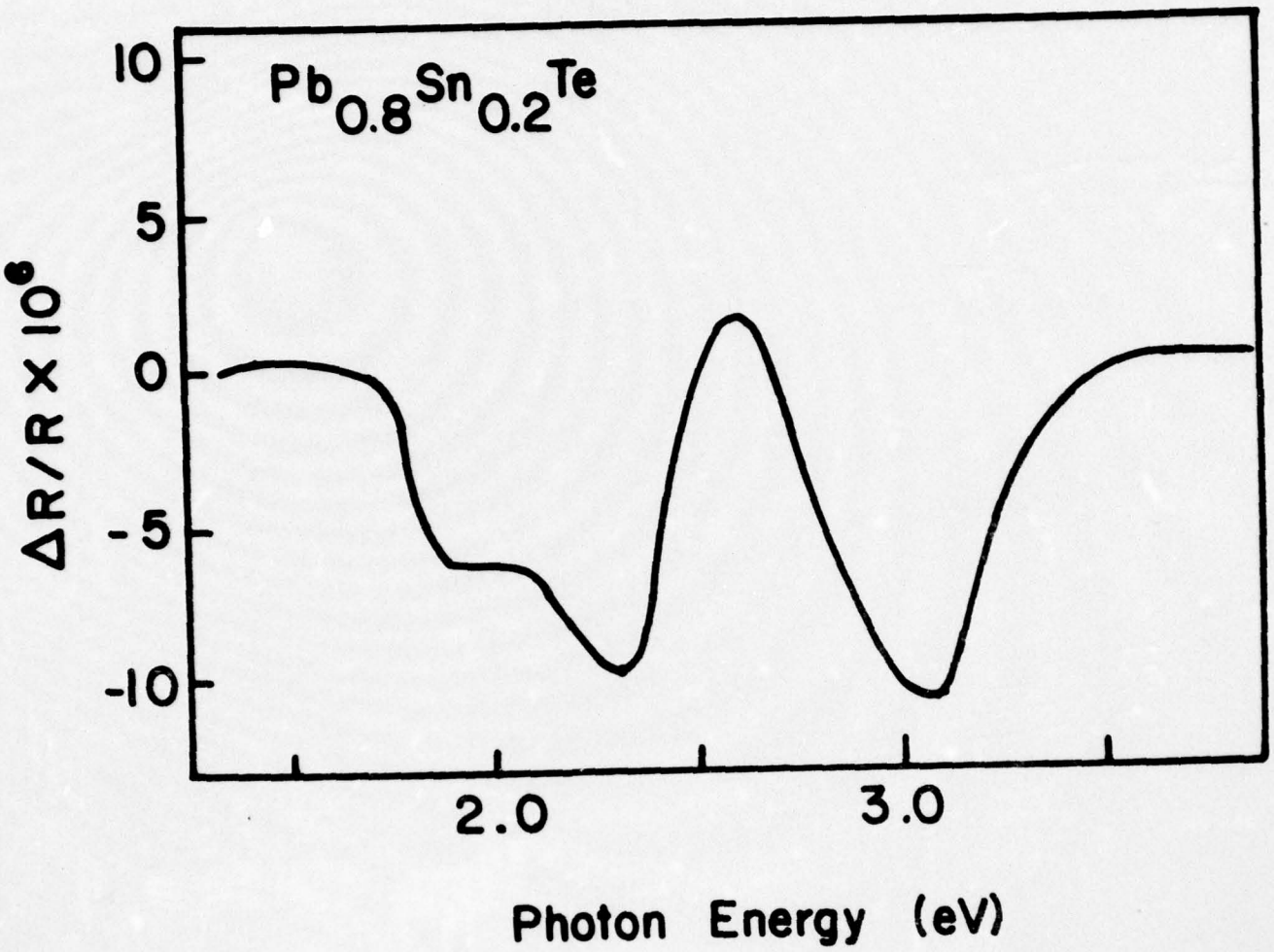

Fig.3. Electroreflectance of $Pb_{0.8}Sn_{0.2}Te$ with a Modulation Square Wave Voltage of +4.5 V/-4.5 V.

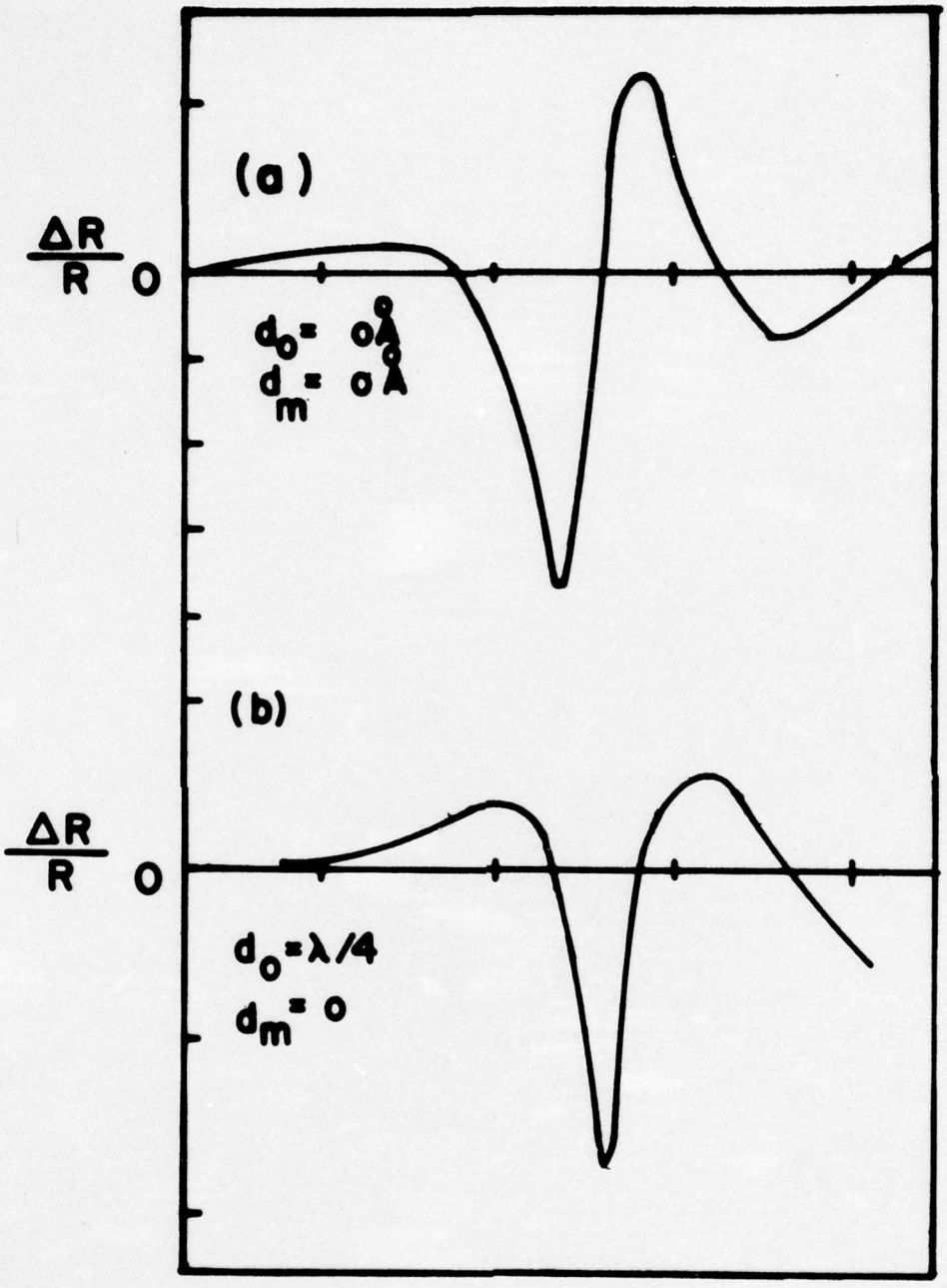

Fig. 4.(a)Electroreflectance Line Shape Without Layers on the Sample Surface. (b)Electroreflectance Line Shape with an Oxide Film Thickness of ¼λ.(13)

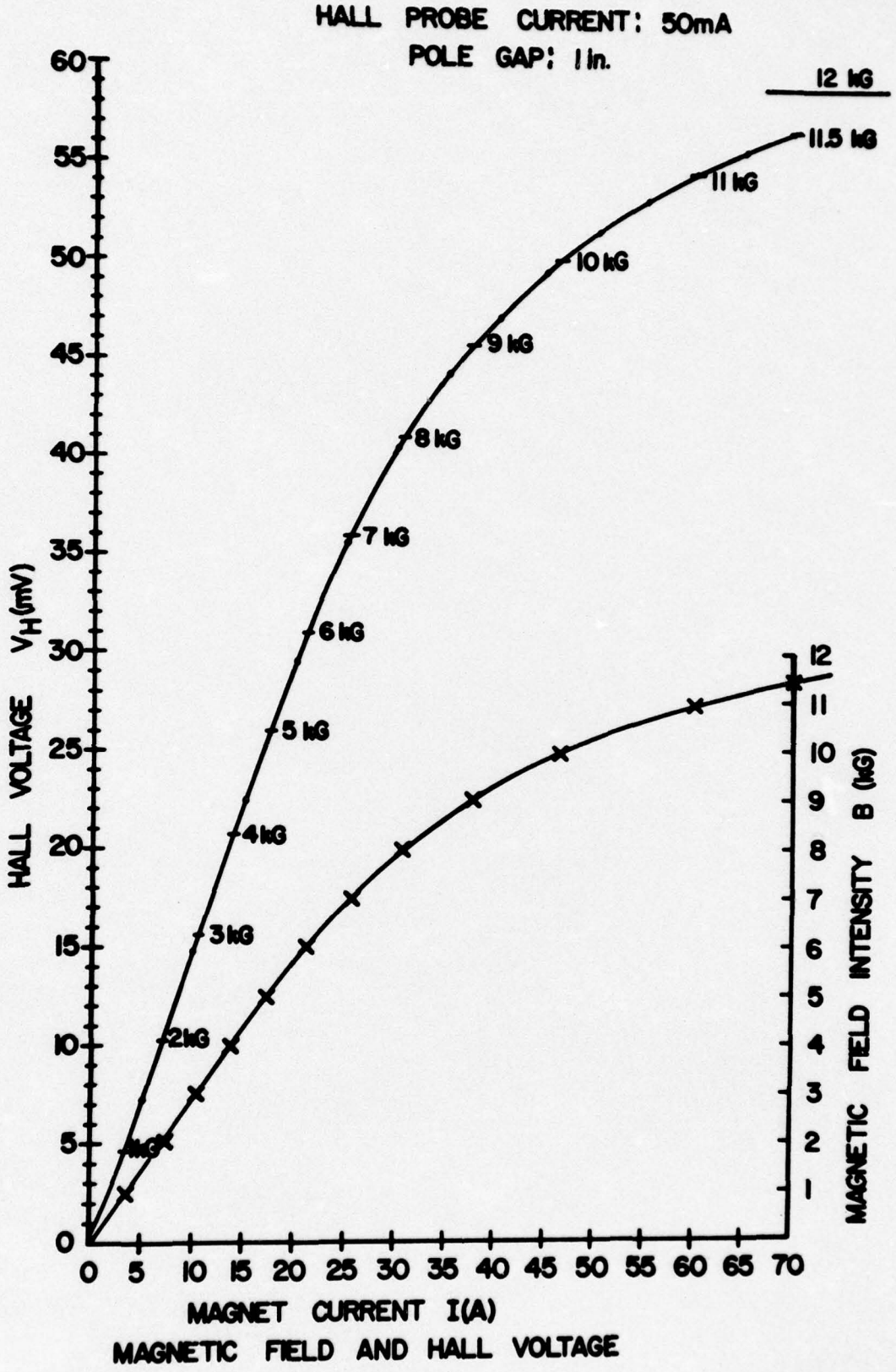
HALL PROBE CURRENT: 50mA
POLE GAP: 1 in.
12 kG
11.5 kG
11 kG
10 kG
9 kG
8 kG
7 kG
6 kG
5 kG
4 kG
3 kG
2 kG
1 kG
HALL VOLTAGE V_H(mV)
MAGNETIC FIELD INTENSITY B (kG)
MAGNET CURRENT I(A)
MAGNETIC FIELD AND HALL VOLTAGE

Fig. 5

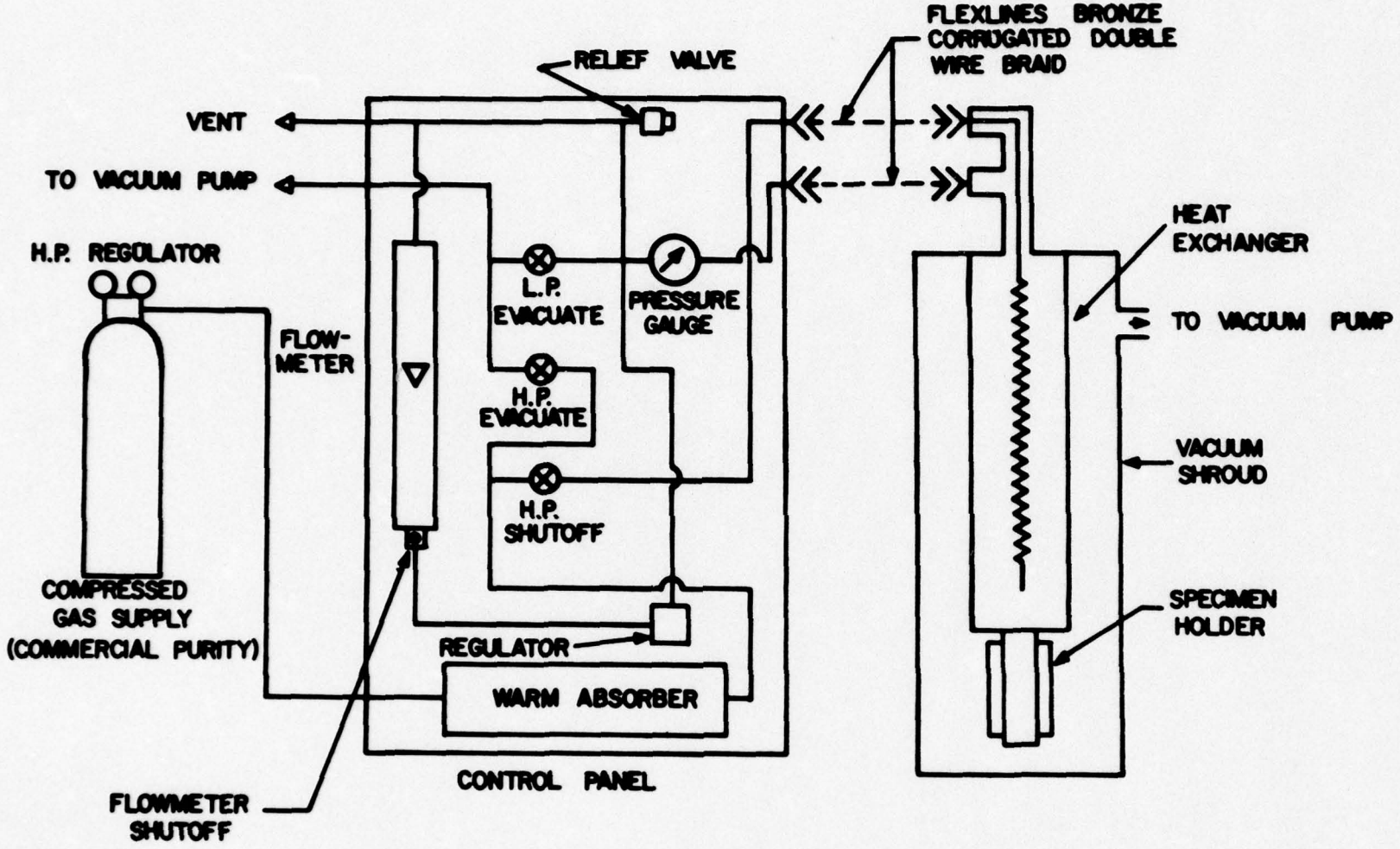

COMPLETE SYSTEM SCHEMATIC FLOW DIAGRAM FOR MINIATURE SINGLE FLUID CRYOSTATS

Fig. 6

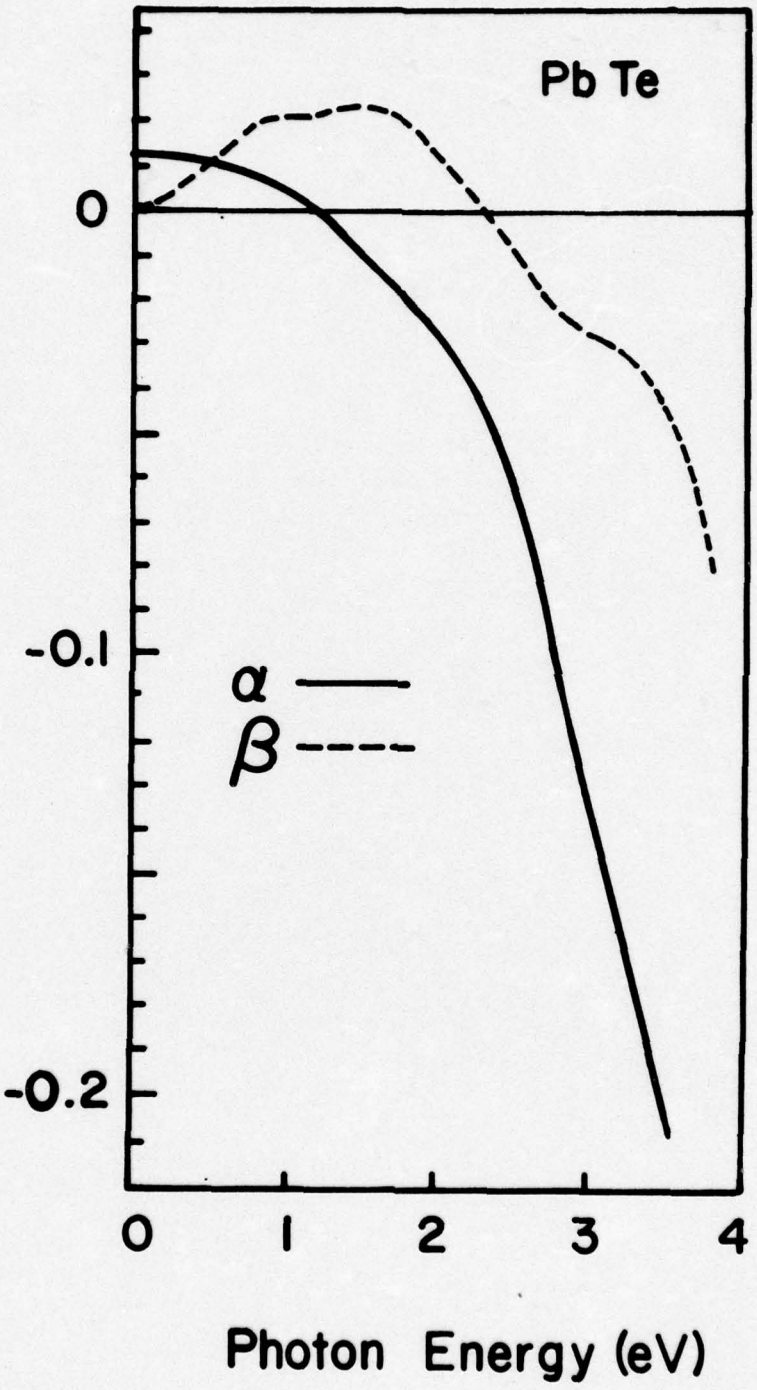

Fig. A-1. α and β of PbTe.[6]

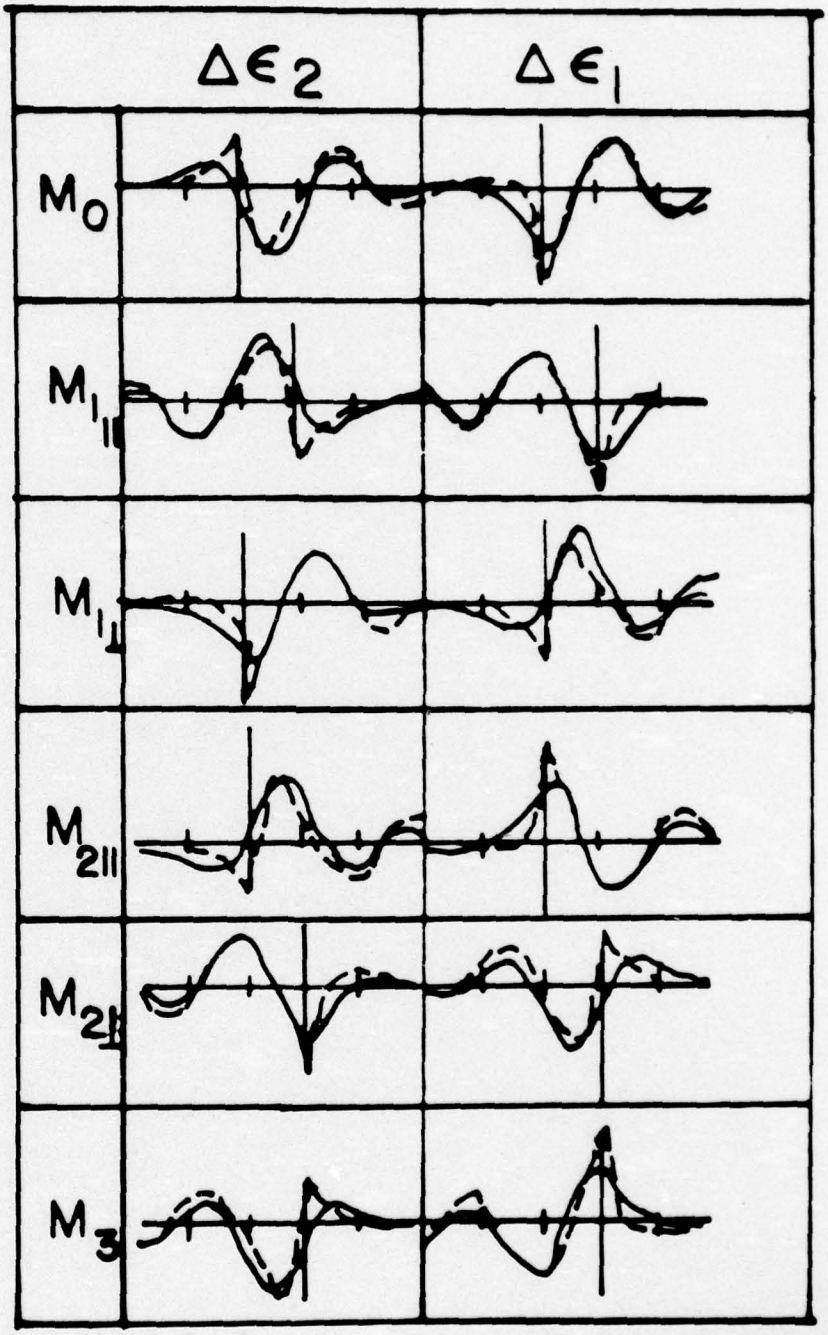

Fig.A-2. Theoretical change of $\Delta\varepsilon_1$ and $\Delta\varepsilon_2$ for the six differenct cases of critical points. The dashed curves are unbroadened. The solid curves correspond to a broadening parameter $\Gamma = 0.5$.

ANNEALING HEATER CIRCUIT CONTROL
(for Pb Sn Te crystals)

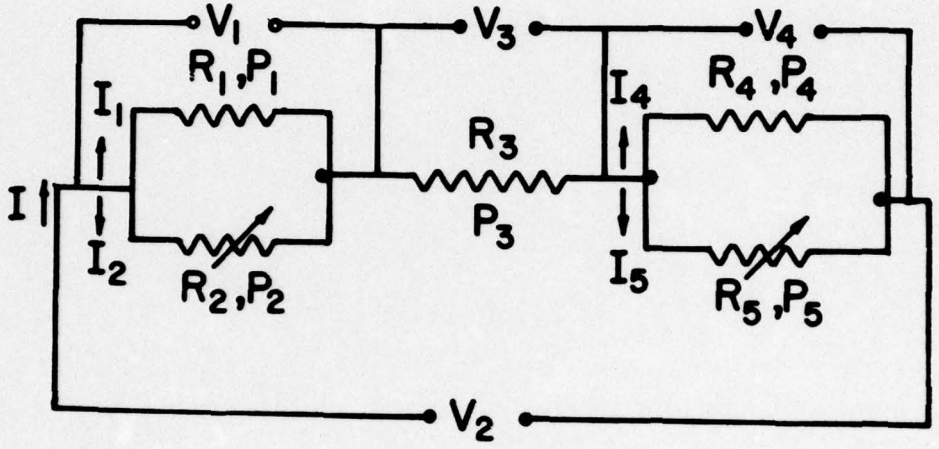

$R_1 = 3.2\,\Omega$

$R_3 = 2.5\,\Omega$

$R_4 = 3.25\,\Omega$

Fig. A-3

APPENDIX A

The relationship between electroreflectance ($\Delta R/R$) (or the field induced change in reflectivity) and the dielectric constant was taken from the derivative of the Freshnel's equations in the form[31]

$$\Delta R/R = \alpha \Delta \varepsilon_1 + \beta \Delta \varepsilon_2 \tag{1}$$

where α and β are functions of dielectric constants ε_1 (real part) and ε_2 (imaginary part) at the photon energy under consideration. α and β are given by

$$\alpha = \frac{\sqrt{2}\varepsilon_s^{1/2}[(\varepsilon_1^2+\varepsilon_2^2)^{1/2}+\varepsilon_1]^{1/2}\ [2\varepsilon_1-(\varepsilon_1^2+\varepsilon_2^2)^{1/2}-\varepsilon_s]}{[(\varepsilon_1-\varepsilon_s)^2+\varepsilon_2^2]\ (\varepsilon_1^2+\varepsilon_2^2)^{1/2}} \tag{2}$$

$$\beta = \frac{\sqrt{2}\varepsilon_s^{1/2}\cdot\varepsilon_2[2\varepsilon_1-(\varepsilon_1^2+\varepsilon_2^2)^{1/2}-\varepsilon_s]}{[(\varepsilon_1-\varepsilon_s)^2+\varepsilon_2^2]\ (\varepsilon_1^2+\varepsilon_2^2)^{1/2}[(\varepsilon_1^2+\varepsilon_2^2)^{1/2}+\varepsilon_1]^{1/2}} \tag{3}$$

where ε_s is the dielectric constant of the surrounding material. The calculated result of α and β in PbTe is shown in Fig. A-1. The field induced change in dielectric constant $\Delta\varepsilon_1$ and $\Delta\varepsilon_2$ has been calculated according to the electro-optical theory as follows:

The imaginary part of the field dependent dielectric function is given by[32]

$$\varepsilon_2(\omega,F) = \frac{e^2|\hat{\varepsilon}\cdot P_{cv}|^2}{\pi m^2 \omega^2} \int_{BZ} dk \frac{1}{|\hbar\Omega(k)|} Ai\left(\frac{E_{cv}(k)-\hbar\omega}{\hbar\Omega(k)}\right) \tag{4}$$

where e is electron charge, $\hat{\varepsilon}$ the unit vector of polarization in the direction of the electric field, P_{cv} the momentum matrix element, m the electron mass. $E_{cv}(k) = E_c - E_v$ (E_c is the energy level of the conduction band; E_v is the energy level of the valence band). Ai(x) is the Airy function defined by $Ai(x) = \int_0^\infty \cos(xt+t^3/3)dt$. The frequency $\Omega(k)$ is defined by

$$\Omega^3(k) = (F\nabla_k)^2 E_{cv}(k)/8\hbar^3 = F^3 8\hbar\mu_F \tag{5}$$

where μ_F is the reduced mass in the direction to the field F. The changes of the imaginary part of the dielectric function $\Delta\varepsilon_2 = \varepsilon_2(\omega,F) - \varepsilon_2(\omega,0)$, have been calculated analytically using the Airy functions for parabolic bands in the effective mass approximation. We consider four types of critical points or transition edges, M_0, M_1, M_2, M_3. The changes in the real part of the dielectric function can be obtained by means of the Kramers-Kronig (KK) relations. The calculated results for $\Delta\varepsilon_2$ and $\Delta\varepsilon_1$ using Eq. (4) and the KK relations for all types of critical points are shown in Fig. A-2. Where $M_{1\parallel}$ and $M_{2\parallel}$ means that the electric field F is parallel to the principal axes of the reduced effective mass, and $M_{1\perp}$ and $M_{2\perp}$ means that F is perpendicular to them. Therefore,

we can analyze the lineshape of the ER data and assign the location of the transitions and the type of critical points as it has been done in Sec. 3. Several other treatments are available with respect to thermal and electrical broadening. The effect of alloy broadening has not been discussed in detail so far and may be interpreted in terms of alloy inhomogeneity.

APPENDIX B

Annealing Heater Circuit Control

The Heater circuit for the annealing oven and its power control arrangement is shown in Fig. A-3. By varying R_2 and R_5 the temperature gradient in the R_3 coil portion of the annealing oven can be controlled precisely. The circuit analysis below is done for the special case of :

R_1 = 3.2 Ohm

R_3 = 2.5 Ohm

R_4 = 3.25 Ohm

and

$P_1 \simeq P_4 \simeq$ 300 Watts

P_3 = 300 Watts.

A null balance proportional temperature controller is used for controlling the heater power precisely. This controller is capable of precisely controlling the power required to maintain the temperature to $\pm$ 0.05°C of the desired set point when controlling resistive heaters ranging from 100 to 3000 Watts.

For the annealing system analysis we use the following relationship between power dissipated and the temperature inside the oven:

$P = CA.T$

where P the power in Watts C the dissipation coefficient in Watts/cm^2.degree, T the temperature in °C, and A the area in cm^2 of dissipation. C depends on air flow rate and surface roughness, therefore $10^{-3} \frac{W}{cm^2 \text{ deg.}} \leq C \leq 3 \times 10^{-3} \frac{W}{cm^2 \text{ deg.}}$. For our purpose we used $C = 10^{-3}$ W/cm^2 °C. The temperature difference T = 700°C. The area of the system is as follows:

$$A = \ell d\pi = 30 \text{ cm. } 5 \text{ cm } \pi = 471 \text{ cm}^2 .$$

For these values, $P = (10^{-3})$ (471) (700°C) = 329.7 Watts. We have assumed negligible radiation and conduction losses. It is desired to produce a small temperature gradient $\leq$ 0.5°C over a sample length of approximately 1 cm. The desired relation is; $P_3 \leq P_1$, P_4; $P_1 = P_4$. This can be achieved by adjustment of R_2 and R_5.

It must now be determined if the resistance of the Heaters will change over the operating range. The following equation defines the effect of temperature on the resistance of a Heater wire:

$$R_T = R_{20}(1 + \alpha\Delta T)$$

where R_T is the resistance at the elevated temperature, R_{20} is the resistance at 20°C, α is the temperature coefficient

and ΔT is the difference in temperature ($\Delta T = T-20$). According to the equation the change in resistance is negligible.

It is now necessary to determine the values of R_2 and R_5 to obtain the desired power dissipation. Assuming $aP_1 = P_3 = aP_4$ where $0.95 \leq a \leq 1$:

$$aI_1^2R_1 = I^2R_3 = aI_4^2 \quad R_4$$

Using $a = 1$

$$I_1 = I\sqrt{\frac{R_3}{R_1}} \; ; \quad I_4 = I\sqrt{\frac{R_3}{R_4}}$$

Using Kirchhoff's laws:

$$I = I_1 + I_2 = I_4 + I_5$$

$$I_2 = I - I_1 \; ; \; I_4 = I - I_5$$

$$I_1R_1 = I_2R_2 \; ; \; R_2 = \frac{R_1I_1}{I_2} \; ;$$

$$I_4R_4 = I_5R_5 \; ; \; R_5 = \frac{R_4I_4}{I_5}$$

$$R_2 = \frac{R_1 I_1}{I_2} = \frac{R_1 I \sqrt{R_3/R_1}}{I - I\sqrt{R_3/R_1}} = \frac{\sqrt{R_3 R_1}}{1 - \sqrt{R_3/R_1}}$$

By similar calculations

$$R_5 = \frac{\sqrt{R_3 R_4}}{1 - \sqrt{R_3/R_4}}$$

$$V_1 = R_1 I_1 = R_1 I \sqrt{R_3/R_1} = I\sqrt{R_3 R1}$$

$$V_3 = R_3 I$$

$$V_4 = I_4 R_4 = I\sqrt{R_3/R_4}, \quad R_4 = I\sqrt{R_3 R_4}$$

Total voltage: $V = V_1 + V_3 + V_4$

$$V = I\left(\sqrt{R_3 R_1} + R_3 + \sqrt{R_3 R_4}\right) = I\sqrt{R_3}\left(\sqrt{R_1} + \sqrt{R_3} + \sqrt{R_4}\right)$$

Total power:

$$P = IV = I^2\sqrt{R_3}\left(\sqrt{R_1} + \sqrt{R_3} + \sqrt{R_4}\right)$$

$$P_1 = V_1 I_1 = R_1 I_1^2 = R_1 I^2 \frac{R_3}{R_1} = I^2 R_3 = P_3 = V_4 I_4 = I_4^2 R_4 =$$

$$I^2 \frac{R_3}{R_4} R_4 = I^2 R_3 .$$

$$P_2 = I_2^2 R_2 = (I-I_1)^2 \; R_2 = \left[I - I\sqrt{R_3/R_1}\right]^2 \left(\frac{\sqrt{R_3R_1}}{1 - \sqrt{R_3/R_1}}\right)$$

$$P_2 = I^2\left(1 - \sqrt{R_3/R_1}\right)^2 \left(\frac{\sqrt{R_3R_1}}{1 - \sqrt{R_2/R_1}}\right) = I^2 \left(1 - \sqrt{R_3/R_1}\right)\sqrt{R_3R_1}$$

$$P_2 = I^2 \left(\sqrt{R_3R_1} - R_3\right) = I^2 \sqrt{R_3}\left(\sqrt{R_1} - \sqrt{R_3}\right)$$

Similarly

$$P_5 = I^2 \sqrt{R_3}\left(\sqrt{R_4} - \sqrt{R_3}\right)$$

Example $P_1 = P_3 = P_4 = 300$ Watts.

$$R_1 = 3.2 \;,\; R_3 = 2.5 \;,\; R_4 = 3.25$$

$$P_3 = R_3 I^2 = 300 \text{ W}$$

$$I = \sqrt{\frac{300\text{W}}{2.5\Omega}} = 10.95\text{A}$$

$$R_2 = \frac{\sqrt{R_3R_1}}{1 - \sqrt{R_3/R_1}} = \frac{\sqrt{2.5 \times 3.2}}{1 - \sqrt{2.5/3.2}} = \frac{2.828}{1-0.8839}$$

$$R_2 = \frac{2.828\Omega}{0.1161} = 24.358\Omega$$

$$R_5 = \frac{\sqrt{R_3 R_4}}{1 - \sqrt{R_3/R_4}} = \frac{\sqrt{2.5 \times 3.25}}{1 - \sqrt{2.5/3.25}} = \frac{2.850}{0.1229} = 23.189$$

Total power:

$$P = I^2 \sqrt{R_3} \left(\sqrt{R_1} + \sqrt{R_3} + \sqrt{R_4}\right)$$

$$P = \left(10.95\right)^2 \sqrt{2.5} \left(\sqrt{3.2} + \sqrt{2.5} + \sqrt{3.25}\right)$$

$$P = 119.9\ A^2\ 1.58\Omega^{1/2}\ (1.788\Omega^{1/2} + 1.581\Omega^{1/2} + 1.8027\Omega^{1/2})$$

$$= 119.9\ A^2\ 1.581\Omega^{1/2}\ [5.1717\Omega^{1/2}]$$

$$P = 980.35W$$

Total voltage:

$$V = V_1 + V_2 + V_3$$

$$V = \frac{P}{I} = \frac{980.35W}{10.95A} = 89.52V$$

$$P_2 = I^2 \sqrt{R_3} \left(\sqrt{R_1} - \sqrt{R_3}\right) - (10.95)^2 \sqrt{2.5\Omega} \left(\sqrt{3.2} - \sqrt{2.5}\right)$$

$$P_2 = 119.9\ A^2\ 1.581\Omega^{1/2}\ [1.7888\Omega^{1/2} - 1.581\Omega^{1/2}]$$

$$P_2 = 119.9\ A^2\ (1.581\Omega^{1/2})\ (0.2078\Omega^{1/2})$$

$$P_2 = 39.39W$$

Similarly

$$P_5 = 40.959$$

Conclusion

These values of the resistors R_2 and R_5 remain the same for various input powers P (for given resistors R_1, R_3, and R_4) and temperature. It has been assumed that $P_1 = P_3 = P_4$. The total power dissipated is $P = 3P_1 + P_2 + P_5$; the effect of temperature on the resistance wires like Manganin, Constantan, and Nichrome is negligible. This is not the case for Iron or Tungsten.

REFERENCES

1. J. O. Dimmock, I. Melngailis, and A. J. Strauss, Phys. Rev. Letters 16, 1193 (1966).
2. B. O. Seraphin, "Electroreflectance" in Semiconductors and Semimetals, Vol. 9, Optical Phenomena, Ed. by R. K. Willardson and R. C. Beer (Academic Press, New York, 1972), pp. 1 - 149.
3. I. Melngailis and T. C. Harman, "Single-Crystal Lead-Tin Chalcogenides" in Semiconductors and Semimetals, Vol. 5, Infrared Detectors, Ed. by R. K. Willardson and R. C. Beer (Academic Press, New York, 1969), pp. 111 - 174.
4. F. Herman, L. C. D. Cuglin, K. F. Cuff, and R. L. Kortum, Phys. Rev. Letters 11, 541 (1963); F. Herman, R. L. Kortum, C. D. Cuglin, R. A. Short, Quantum Theory of Atoms, Molecules, and the Solid State (Academic Press, New York, 1966), p. 381.
   L. E. Johnson, J. B. Conklin, G. W. Pratt, Jr., Phys. Rev. Letters 11, 538 (1963); G. W. Pratt, Jr., Quantum Theory of Atoms, Molecules, and the Solid State (Academic Press, New York, 1966), p. 429.
5. I. Melngailis, Journal de Physique (Supplement N^{O} 11-12) 29, C4-84 (1968).
6. H. Piller, "Faraday Rotation" in Semiconductors and Semimetals, Vol. 8, Transport and Optical Phenomena, Ed. by R. K. Willardson and R. C. Beer (Academic Press, New York, 1972), pp. 103 - 181.

7. H. Piller, Proc. of the 7th International Conference on the Physics of Semiconductors, Paris, 297 (1964).

8. C. J. Summers and S. D. Smith, Proc. Physical Society 92, 215 (1957).

9. W. Thielemann, Phys. Stat. Sol., 34, 519 (1969).

10. D. L. Mitchell, E. D. Palik, and R. F. Wallis, Phys. Rev. Letters 14, 827 (1965).

11. D. L. Mitchell, E. D. Palik, and R. F. Wallis, Proc. International Conference on the Physics of Semiconductors. Kyoto, 197, (1966).

12. E. Burstein, G. S. Picus, R. F. Wallis, and F. Blatt, Phys. Rev. 113, 15 (1969).

13. I. M. Boswarva, R. E. Howard, and A. B. Lidiard, Proc. Roy. Soc. A269, 125 (1962). H. S. Bennett, E. A. Stern, Phys. Rev. 137, 448 (1965).

14. F. F. Sizov, G. V. Lashkarev, V. B. Orletskii, and E. T. Grigorovich, Sov. Phys. Semicond., Vol. 8, No. 11.

15. Yu. I. Ukhanov, Sov. Phys. - Usp., Vol. 16, No. 2, pp. 236 - 249.

16. I. A. Chernik, V. I. Kaidanov, M. I. Vinogradova, and N. V. Kolomoets, Sov. Phys. Semicond., 2, 645 (1968).

17. G. V. Lashkarev, D. F. Miglei, K. D. Tovstyuk, and A. D. Shevchenko, Sov. Phys. Semicond. 8, 929 (1975).

18. T. C. Harman and J. P. McVette, J. Electronic Materials 3 843 (1974).

19. R. F. Brebrick, J. Phys. Chem. Sol. 24, 27 (1963).

20. D. G. Coats, J. Electrochem. Soc. 108, 1038 (1961).

21. J. E. Fisher, Rev. Sci. Instr. 42, 872 (1971).

22. D. E. Aspnes and M. Cardona, Phys. Rev. 173, 714 (1968).

23. The energy band structure and the assignment of marks are shown in References (22), (24), and (26).

24. F. J. Bogacki, A. K. Sood, C. Y. Yang, S. Rabii and J. E. Fisher, Surface Science 37, 494 (1973).

25. M. Cardona and D. L. Greenway, Phys. Rev. 133, A1685 (1964).

26. P. J. Lin and L. Kleinman, Phys. Rev. 142, 478 (1966).

27. R. Glosser and B. O. Seraphin, Phys. Rev. 187, 1021 (1969).

28. J. B. Conlin, Phys. Rev. 137, A1282 (1964).

29. O. Berolo, Spin-orbit splitting in III-V alloys, Ph.D. Thesis, University of Ottawa, Canada.

30. D. E. Aspnes, Surface Science 37, 418 (1973).

31. B. O. Seraphin and R. B. Hess, Phys. Rev. Letters 14, 138 (1965); B. O. Seraphin and N. Bottka, Phys. Rev. 145, 628 (1966).

32. D. E. Aspnes, P. Handler and D. F. Blossey, Phys. Rev. 166, 921 (1968).

33. M. Cardona, "Modulation Spectroscopy" Suppl. 11 to Solid State Physics (Academic Press, New York, 1969).

34. L. van der Pauw, Philips Res. Rept. 13, 1 (1958).